Biochimica et Biophysica Acta 1848 (2015) 1092–1098

Contents lists available at ScienceDirect

Biochimica et Biophysica Acta

journal homepage: www.elsevier.com/locate/bbamem

Effects of ursolic acid on the structural and morphological behaviours of dipalmitoyl lecithin vesicles

András Lőrincz, Judith Mihály, Csaba Németh, András Wacha, Attila Bóta *

Research Centre for Natural Sciences, Hungarian Academy of Sciences, Institute of Materials and Environmental Chemistry, Research Group of Biological Nanochemistry, 1117 Budapest, Magyar tudósok körútja 2, Hungary

ARTICLE INFO

Article history:
Received 28 July 2014
Received in revised form 12 November 2014
Accepted 12 January 2015
Available online 22 January 2015

Keywords:
Ursolic acid
Non-bilayer lipid structure
DPPC
Small- and wide-angle X-ray scattering (SWAXS)
Freeze-fractured transmission electron-microscopy (FF-TEM)

ABSTRACT

Effects of ursolic acid on the structural and morphological characteristics of dipalmitoyl lecithin(DPPC)-water system was studied by using differential scanning calorimetry (DSC), small- and wide-angle X-ray scattering (SWAXS), freeze-fracture method combined with transmission electron-microscopy (FF-TEM) and infrared spectroscopy (FT-IR). The surface of the uncorrelated lipid system is rippled or grained and a huge number of small, presumably unilamellar vesicles are present if the UA/DPPC molar ratio is 0.1 mol/mol or higher. Besides the destroyed layer packing of regular multilamellar vesicles, non-bilayer (e.g. cubic or hexagonal) local structures are evidenced by SAXS and FF-TEM methods. The ability of UA to induce non-bilayer structures in hydrated DPPC system originates from the actual geometry form of associated lipid and UA molecules as concluded from the FT-IR measurements and theoretical calculations. Beside numerous beneficial e.g. chemopreventive and chemotherapeutic effect of ursolic acid against cancer, their impact to modify the lipid bilayers can be utilized in liposomal formulations.

1. Introduction

Ursolic acid (UA) is a plant-derived triterpenic molecule which can be found in several spices and fruits. It is known that ursolic acid induces apoptosis in tumor cells and is a substrate of multidrug resistance proteins [1–4]. This pentacyclic triterpenoid has gained much attention by its chemopreventive and chemotherapeutic effect against cancer [5,6]. It has been proven that it targets multiple proinflammatory transcription factors, cell cycle proteins, and other important molecules related to cell signalling. UA has been recognised to influence an apoptosis, angiogenesis and proliferation by affecting different signal transduction molecules [7]. Triterpenoids have a known effect in the prevention and therapy of many diseases, and some have already been in Phase I clinical trial [8]. Consequently, the intake of UA into the human body favours medical purpose. However, its effects on different cell organisms are not known in details. Studies on model membrane systems (e.g. multilamellar vesicles) can provide primary information about the impact of UA on the lipid bilayer structure [9–12]. Prades et al. have presented results on the modulated structures of multilamellar 1,2-dipalmitoylphosphatidylcholine (DPPC) – water systems induced by three different triterpenic acids (TTPs), UA among them [11]. They have reported that the TTPs does not destabilize the lipid bilayers in gel ($L_{\beta'}$) phase, while layered and non-bilayer isotropic structures (presumably "inverted micelles") were present in the temperature domain of the liquid crystalline (L_{α}) phase. Here we report unambiguous experimental facts which help to describe the wealthy of the structural and morphological formations in hydrated lipid – UA mixtures. These findings indicate severe changes in the bilayer self-organization, whereby significant perturbations in biological membranes can be hypothesized.

We have used fully hydrated multilamellar DPPC – water vesicles to observe structural changes in this model membrane system induced by the presence of UA. Moreover, the structural and morphological features, thus revealed, can be utilized to develop nanocarrier systems (e.g. small unilamellar vesicles) used in clinical practice [13]. For a comprehensive study we have used differential scanning calorimetry (DSC), whereby the thermal characterization of the system, e.g. the changes in enthalpy and the phase transition temperatures can be deduced [14]. The scattering methods identify the structure: small-angle X-ray scattering (SAXS) distinguishes between lamellar and non lamellar structural formations [15], wide angle X-ray scattering (WAXS) profiles provide information about the subcells in the chain regions of the lipids [16]. The freeze-fracture method combined with transmission electron-microscopy (FF-TEM) yields direct visual information about the morphological formations whereby the interpretation of SAXS curves is supported [17]. Infrared spectroscopy (IR) is used to study the fine structures of the constituents. Changes in the frequencies and profiles of vibrational bands provide the information on the interactions between the host and guest molecules, while theoretical calculations

* Corresponding author. Tel.: +36 1 382 6427.
E-mail address: bota.attila@ttk.mta.hu (A. Bóta).

http://dx.doi.org/10.1016/j.bbamem.2015.01.010
0005-2736/

give direct explanations for configurations and molecular interactions [18,19].

2. Materials and methods

2.1. Materials

High purity synthetic 1,2-dipalmitoyl-sn-glycero-3-phosphocholine (DPPC, or with other term dipalmitoyl lecithin) was purchased from the NOF Corporation (Japan). The ursolic acid (UA) was purchased from Sigma Aldrich (>98,5%). All materials were used without further purification. Appropriate amounts of the lipid (DPPC) and the powder of UA were mixed and dissolved in chloroform containing 30 vol% methanol. The solution was evaporated at room temperature, and then the resulting solid UA-lipid film was kept in vacuum for 8 hours to remove the residual traces of solvent. The mixtures of lipid and UA were hydrated in MilliQ water to achieve 20 wt% lipid contents. Different samples were prepared at 0.01, 0.1, 0.2, and 0.3 UA/DPPC molar ratios. In all cases, hydration was followed by freeze-thaw cycle: Starting with heating to 50 °C, followed by cooling to 4 °C, and reheating to 50 °C, while intensive vortexing applied. This procedure was repeated more than twenty times to achieve homogeneous dispersions.

2.2. Differential scanning calorimetry (DSC)

Samples were examined with a Setaram μDSC3 evo apparatus. All samples were scanned at least three times from 20 °C to 60 °C. The scan rates were initially 1 °C/min, and 0.5 °C/min during the heating period, as well as 1 °C/min during the cooling period. An empty sample holder was used as a reference. The quantities of the samples used for the DSC measurements were approximately 10 mg.

2.3. Small- and wide-angle X-ray scattering (SAXS, WAXS)

Small- and wide-angle X-ray scattering measurements were performed using a modified compact Kratky-type camera with slit collimation. The SAXS intensity curves were corrected by considering the geometry of the beam profile based on the direct desmearing method described by Singh et al. [20]. The X-ray source was a Cu-anode sealed X-ray tube. The scattering of Ni-filtered CuKα radiation ($\lambda = 0.1.542$ nm) was recorded in the small-angle range from $q = 6{\cdot}10^{-2}$ to 6 1/nm. The scattering variable is defined as $q = 4\pi{\cdot}\sin\Theta/\lambda$, where 2Θ is the scattering angle with the relationship $q = 2\pi/d$, where d is a characteristic periodicity in the sample. Thin-walled quartz capillaries with an average diameter of 1 mm were filled with the samples. The capillary containing the sample under study was inserted into a metal capillary holder, which was then placed into an aluminium block. To perform the measurements, this block was positioned directly in the beam line, and it was used as a thermal mass for controlled temperatures. X-ray measurements were performed after 15 min incubation at the respective temperatures. The exposure time was 3600 s in each case by using two MBraun PSD-50 type linear position selective detectors (MBraun, Garching, Germany) in the small- and wide-angle regimes, respectively.

2.4. Freeze-fracture transmission electron microscopy (FF-TEM).

For freeze-fracture (FF) experiments, droplets of 1-2 μL of the sample were pipetted onto a gold sample holder and frozen by plunging it immediately into partially solidified freon for 20 s and stored in liquid nitrogen. Fracturing was performed at -100 °C in a Balzers freeze-fracture device (Balzers BAF 400D, Balzers AG, Liechtenstein). Replicas of the fractured faces etched at -100 °C for 20 sec. were made by platinum-carbon shadowing and then cleaned with a water solution of surfactant and washed with distilled water. The replicas were placed on 200 mesh copper grids and examined in a MORGAGNI 268D (FEI, The Netherlands) transmission electron microscope.

2.5. Fourier transform infrared spectroscopy (FT-IR)

FT-IR spectra were recorded using attenuated total reflection (ATR) technique by a Varian 2000 FT-IR spectrometer (Scimitar Series) fitted with a 'GoldenGate' single reflection diamond ATR unit (Specac Ltd., UK). A home-made liquid cell was applied for temperature controlled measurements. Approximately 5 μL of liposome dispersions were spread on the top of the ATR element and the temperature was equilibrated for 5 min before acquisition of each spectrum; 128 scans were cumulated at a nominal resolution of 2 cm^{-1}. ATR correction and water background spectral subtraction was performed after each data collection. The actual frequencies of complex IR bands were determined by fitting their peaks to Lorentzian curves. For all spectral manipulation, the Grams/32 software package (Galactic Inc., USA) was used.

2.6. Theoretical calculation

The quantum chemical calculations were performed with the Gaussian03 program package [21]. Density functional theory (DFT) method with the b3lyp/6-31 g(d) basis sets [22] was used to estimate equilibrium geometries, energies, as well as frequencies (to model infrared spectra). We also emphasize that calculation is snapshots of a stable configuration part from a certain domain, but not on the entire vesicle.

3. Results

3.1. Thermotropic features of the hydrated DPPC and UA mixture

The fully hydrated DPPC system undergoes two phase transitions in the investigated temperature domain. These are the pretransition between the gel and rippled gel phases (approximately at 34 °C) and the main transition between the rippled gel and liquid crystalline phases (at 41 °C). The pretransition exhibits a weak first order phase transition character compared to the main transition. Strong fluctuations can be occurred in the whole system whereby the effect of guest molecules becomes stronger than during the chain melting transition [23]. The pre- and main transitions are accompanied by a significant change in enthalpy, as shown in Supplement (S1). At UA/DPPC = 0.01 mol/mol ratio, UA induces only a small perturbation in the thermal behavior of the system (Fig. 1). By increasing the ratio of UA the changes in enthalpy decrease in case of both the pre- and main transitions. The shape of the signal of the main transition is strongly altered. The broadening of the characteristic signal of chain melting is caused by the decrease of the cooperativity of the lipid molecules during phase transition. The small peak, characteristic for the pure system, indicates the presence of domains without UA and in the same time shows a limited miscibility of UA molecules in the lipid matrix. The wide shoulder in the right side of the transition signal is caused by domains rich in UA guest molecules. In the increased UA concentration regime (UA/DPPC = 0.1; 0.2; 0.3) the shoulder became dominant. Similar effect was observed by Prades et al. [11]. Presumably, the domains rich in UA are thermodynamically stable creations because of the positive shift of the chain melting. By increased UA concentration the thermodynamic differences between the thermally adjacent parent phases vanish indicating the strong structural effect of the guest molecules in the self-organization.

3.2. UA induced nanostructural formations

The periodic multilayered-arrangement of the DPPC vesicles is evidenced by small angle X-ray scattering (or more exactly by small angle X-ray diffraction, SAXD) since Bragg reflections appear in several orders on the small angle scattering patterns of the vesicles. The periodic distance of the fully hydrated DPPC-water system, corresponding to

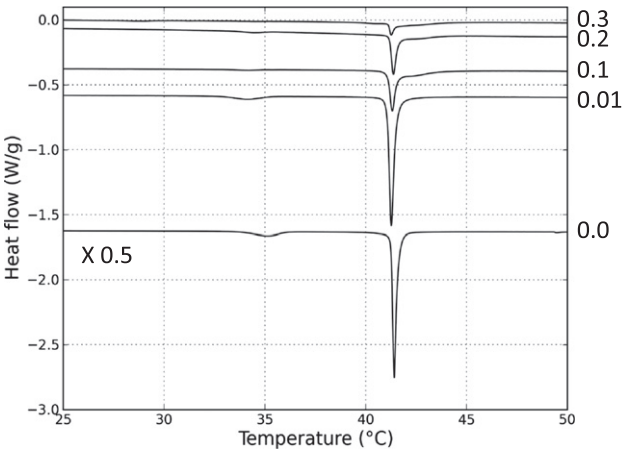

Fig. 1. DSC thermograms of 20 wt% fully hydrated DPPC systems. UA/DPPC molar ratios of the systems are denoted in the figure (the basic lines of thermograms are shifted along the *y* axes). The characteristic data (changes in enthalpy, transition temperatures) are summarized in Supplement (Table 1).

the lipid bilayer and the water shell, is characteristic for the different lyotropic mesophases, i.e. 6.4 nm in gel ($L_{\beta'}$), 7.1 nm in rippled gel ($P_{\beta'}$) and 6.7 nm in liquid crystalline (L_α) phases.

The presence of UA results in a distortion of the layer structure of the system as it is found from the shape of the one-dimensional SAXS curves shown in Fig. 2. The changes in the Bragg reflection profiles, with respect to that of the hydrated DPPC system, indicate the effect of UA concentration on the one-dimensional layer-arrangement in all the three characteristic temperature domains at 25 °C, 38 °C and 46 °C, corresponding to the gel, rippled gel and liquid crystalline phases of the pure lipid system, respectively.

The dominant Bragg reflections appear at least in two orders located at the values of scattering variables of $q_1 = 2\pi/d$ and $q_2 = 4\pi/d$, where d is the periodicity (given above for the three mesophases) indicating that the lamellar structure is characteristic for the systems without UA or containing UA in low concentration (UA/DPPC = 0.01). The broad wide angle scattering signals of lipid subcell (not shown here) exhibit the perturbed chain packing in the temperature domain of gel phases in accordance with other published data [11]. In high UA concentration regime the guest molecules destroy the lamellar structure in all the three characteristic temperature domains as shown by the extremely broadened Bragg reflections. According to the alterations in SAXS pattern, the rippled gel phase (38 °C) was the most sensitive to the presence of UA, showing a preferred location of the UA molecules close to the lipid-head region. (These structural changes may induce the reduction of cooperativity during the phase transition observed by DSC method.) Drastic changes occur in the scattering patterns if the UA/DPPC molar ratio is 0.1 mol/mol or higher. The scattering curves turns into a non-characteristic form, without any pronounced diffraction peak, indicating the sparse occurrence of domains with stacks of lamellae and the abundance of amorphous nanostructures. Moreover, the positions of diffuse Bragg reflections of the systems with 0.2 and 0.3 mol/mol UA/DPPC molar ratios do not follow the characteristic equidistant alignment of the periodical layer arrangement, indicating the local formations of non-layered (e.g. cubic or hexagonal) and in the same time rather amorphous structures. Taking into account the effect of the temperature, it is worth to mention that the layer structure, followed by its first Bragg reflection, characteristic above the chain melting temperature, is most dominant in even at 0.3 mol/mol UA/DPPC molar ratio.

The described changes in the reciprocal space refer to a severe loss in the layer correlation, and to local formations of non-lamellar structures. On the other hand, no information can be deduced about the formations of uncorrelated bilayers. The method of FF-TEM provides an excellent opportunity to identify these types of formations. A fully hydrated pure DPPC system consists of nearly spherical multilamellar vesicles. The self–organization, however, causes polydispersity as it can be directly visualized in FF-electronmicrographs. The typical diameter of vesicles ranges from hundreds of nanometers up to several micrometers. The existence of the periodicity is observable, but the precise value of the repeating distance cannot be determined because the uncertainty introduced in the fracturing process. We present the surface morphology of the system with 0.2 mol/mol UA/DPPC molar ratio in Figs. 3,4. The peculiar formations on the nanometric scale clearly show the structural defects compared to the regular multilayer packing in the pure DPPC–water system. These, and even more, the non-layer formations, indicate the ability of UA to drastically perturbate the characteristic nanostructure of the DPPC-water system.

In the pictures the non-regular morphology is typical, large and nearly spherical multilamellar vesicles appear occasionally (Fig. 3/A). Surprisingly, there is no trace of laterally extended sheets of bilayers which are typical morphologies of uncorrelated hydrated lipid systems

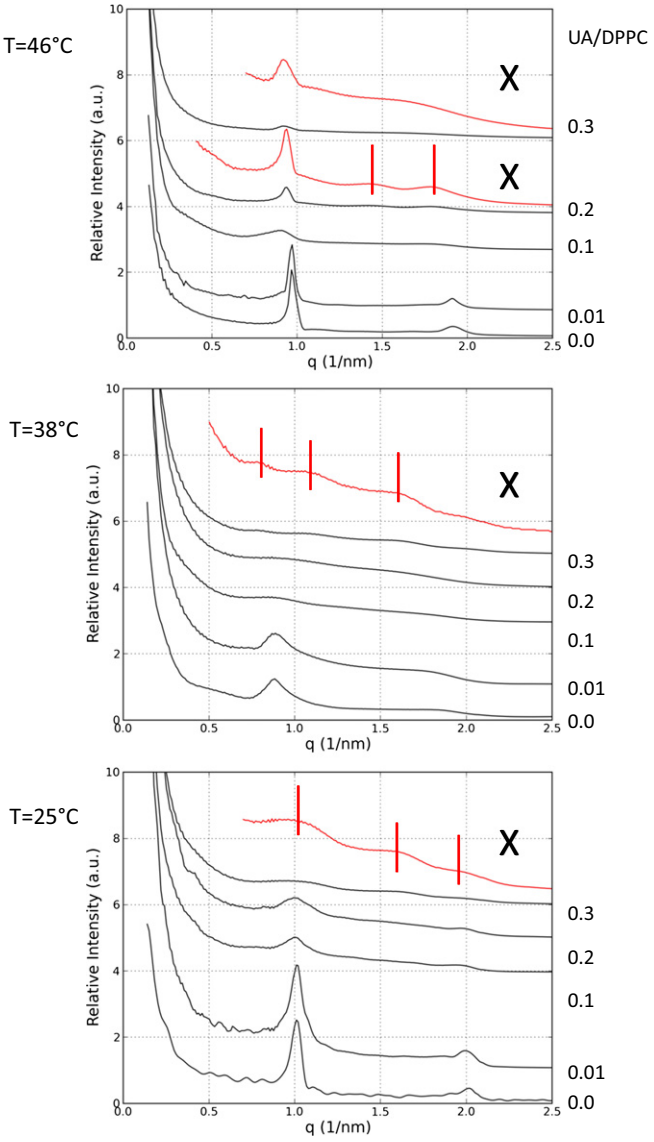

Fig. 2. SAXS patterns of 20 wt% fully hydrated DPPC systems in gel, rippled gel and liquid crystalline phases at 25, 38 and 46 °C, respectively. UA/DPPC molar ratios of the systems are denoted in the figure.

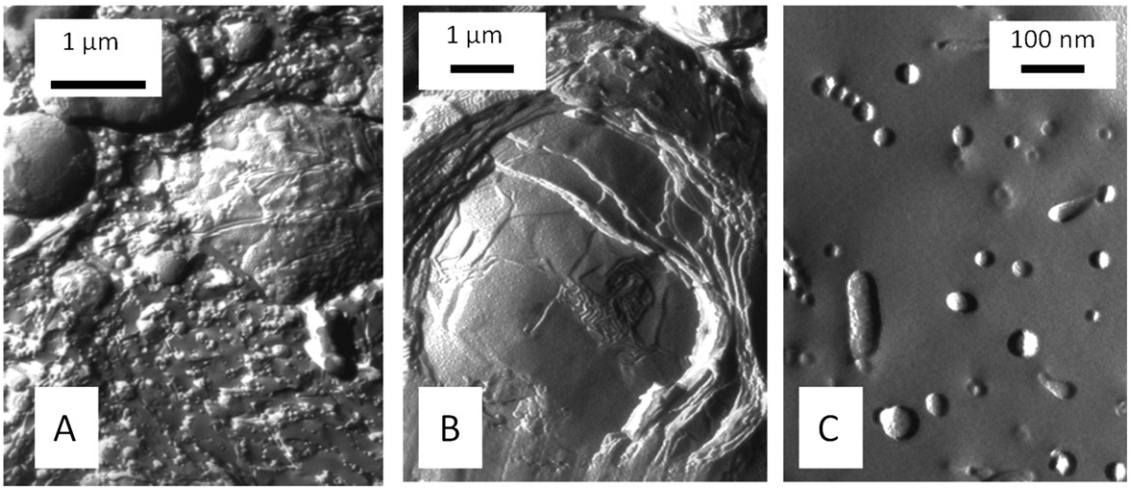

Fig. 3. Surface morphologies of the layer formations in 20 wt% fully hydrated DPPC system with 0.2 mol/mol UA/DPPC molar ratio. Non-regular morphology is typical, spherical multilamellar vesicles appear occasionally (A), surface of the layers is rippled or grained (B), huge number of small particles (<100 nm) (C).

[24]. The surface of the layers are rather rippled or grained as shown in Fig. 3/B. Apart from these polydisperse multilamellar creations, a huge number of small particles are visible, which are the most dominant creations in the sample. Their main diameter falls into the size range below 50 nm as demonstrated in Fig. 3/C. Considering the small radii of their layer curvature they are expected to be unilamellar vesicles.

Besides the above mentioned spherical formations, two types of morphological features are present: Stacks of closely packed and parallel, as well as elongated, worm like creations can be observed in Fig. 4/A. The thickness of elongated units can be approximated to be cca. 12 nm. The other type exhibits also closely packed, nearly isotropic grains as it can be observed in Fig. 4/B. Transitional shapes between these two types can also be found (Fig. 4/C) indicating the transformation between these forms. This visual information provides explanation for non–lamellar formations. The domains containing elongated units and grains correspond to hexagonal and cubic structures, respectively.

3.3. Guest-host interactions on atomic scale

FT-IR spectra of UA loaded DPPC systems with different concentrations of UA were recorded at room temperature (25 °C) shown in Fig. 5. For comparison, the spectrum of pure DPPC is presented, too. The main spectral difference observed due to the presence of UA is a new band around 1691 cm^{-1} (Fig. 5). These small bands in the spectra of UA-DPPC systems observed at 0.1, 0.2 and 0.3 UA/DPPC molar ratios suggest that a part of UA is in aggregated, presumably in mainly dimer form. Teixeira et al. [25] studying mixed monolayers of oleanolic acid (isomeric analog of UA) and stearic acid have also observed that oleanolic acid molecules form dimers as in pure phase of oleanolic acid, and this interaction prevails over the oleanolic-water hydrogen bonds. Moreover, the presence of UA in form of aggregates is in accordance with the very poor water-solubility of UA, limiting its direct use in medical applications [26]. This band assignment above was also tested by detailed spectroscopic IR measurement and *ab initio* calculations on pure UA. The IR spectrum of solid UA exhibits two overlapped bands at 1711 cm^{-1} and 1685 cm^{-1} (see Supplement S2). The band at 1711 cm^{-1} is associated with C = O stretching from acid monomers, while the 1685 cm^{-1} band can be associated with aggregated species, suggesting that a huge part of UA is in form of dimers and/or aggregates. Comparison with simulated spectra obtained as the result of *ab initio* calculations using density functional theory (DFT) method (Gaussian 03, B3LYP method and 6-31 G(d) basis set; scaled frequency with quadratic scaling equation) [21] the presence of UA aggregates is also consolidated.

The polar headgroup vibrations of DPPC molecules are represented by the antisymmetric stretching of the PO_2^- groups (1223 cm^{-1}),

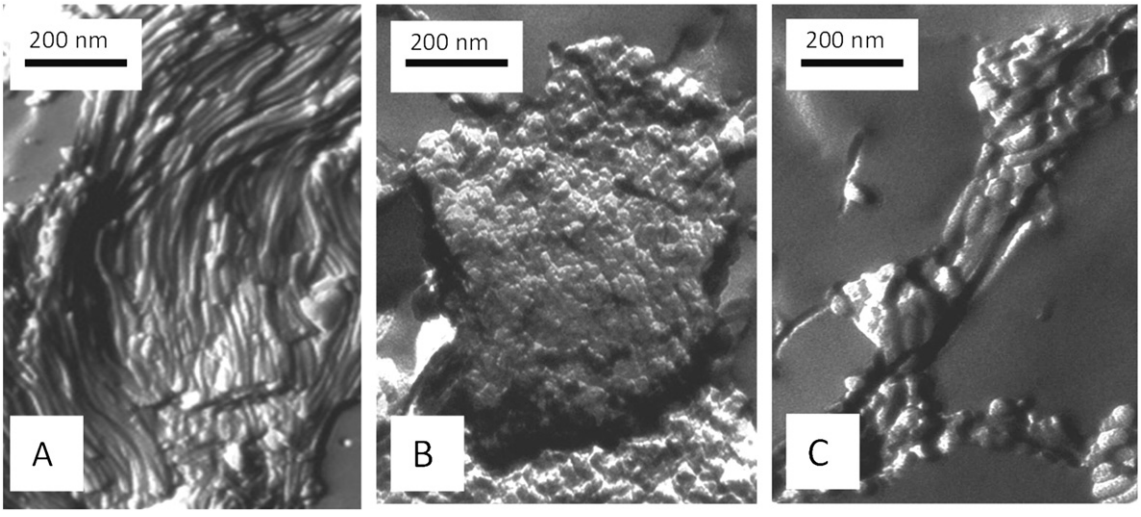

Fig. 4. Surface morphologies of the non-lamellar formations in 20 wt% fully hydrated DPPC system with 0.2 mol/mol UA/DPPC molar ratio. Closely packed and elongated, worm like creations (A), closely packed, nearly isotropic grains (B), transitional shapes between the elongated and isotropic types (C).

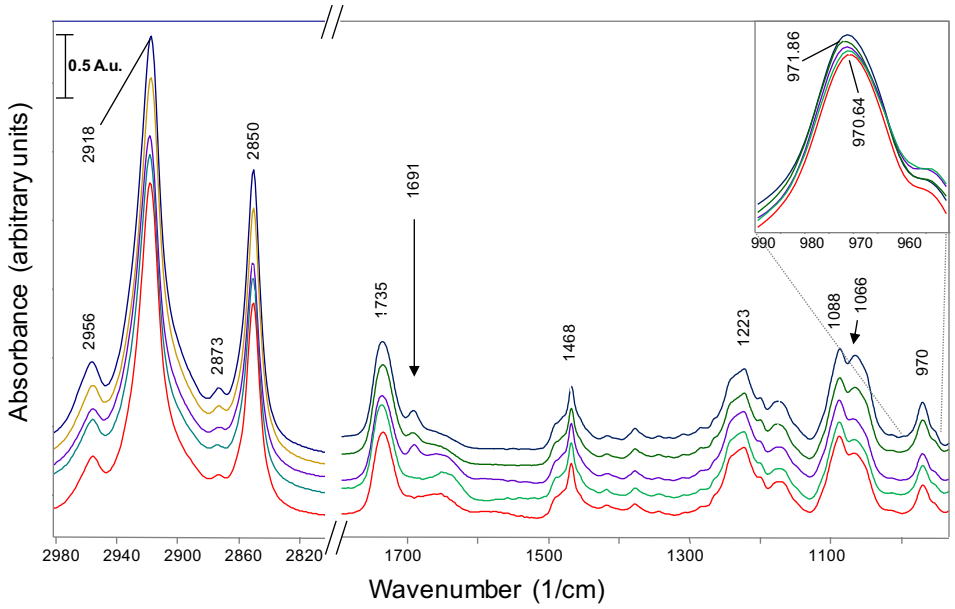

Fig. 5. FTIR spectra (after water subtraction) of 20 wt% fully hydrated DPPC systems recorded at room temperature (25 °C). From bottom to top: pure DPPC system; UA loaded DPPC systems with 0.01, 0.1, 0.2 and 0.3 UA/DPPC molar ratios.

symmetric PO_2^- stretching (1088 cm^{-1}) partially overlapped with the band belonging to the C–O–P–O–C stretching modes (1066 cm^{-1}) [27] and the band representing the antisymmetric C-N^+ stretching vibrations (971 cm^{-1}) of the choline groups [28] (see Fig. 5). The position of ν_{as}C-N^+ vibration is sensitive only to the presence of UA (Fig. 5, inset). The slight shift of ν_{as}C-N^+ can be explained as follows: no H-bonding is supposed to form between the positively charged $(CH_3)_3$-N^+ group and water. However, water molecules are expected to associate with choline groups in hydrated DPPC through weak polar interactions. The presence of 0.1-0.3 mol/mol UA/DPPC might change this 'solvent effect' [29].

The carbonyl ester group is located in the interfacial region of the lipid bilayer and is a potential H-bonding formation site. In the FT-IR spectra of hydrated DPPC bilayers the carbonyl stretching band (νC = O) occurs around 1735 cm^{-1}. In highly hydrated bilayers this band splits in two overlapping components: a high wavenumber band around 1742 cm^{-1} of the non-hydrogen bonded C = O groups and a low wavenumber band around 1728 cm^{-1} due to the hydrogen bonding of the C = O groups [30]. The exact positions of these bands are affected also by the geometry of glycerol moieties and the packing of the acyl chains. Fig. 6 shows the quantitative analysis of the carbonyl interactions presented by the ratio of the two component bands. (Band positions were estimated via the second derivatives, and band shapes were approximated by Lorentzian function with minimizing the statistical parameter χ^2 until it became minimal.) The relative amount of H-bonding to the lipid C = O groups is decreased by the presence of UA molecules. It seems plausible that the dimers and/or aggregates of UA reside in the interfacial region of the lipid bilayer and displace water molecules from the so called 'secondary hydration shell' of the lipid molecules [31]. To confirm this statement, the same FT-IR measurement was repeated on anhydrous lipids (dry film spectra), and no change in the ratios of the two component bands was witnessed, which excludes the existence of direct interactions between the C = O groups and guest molecules.

Fig. 7 shows the temperature dependence of the wavenumber of the symmetric CH_2 stretching mode for UA-DPPC liposomes. The abrupt increase in the peak frequency is due to the change from *trans* to *gauche* conformers of acyl chains during the main endothermic phase transition

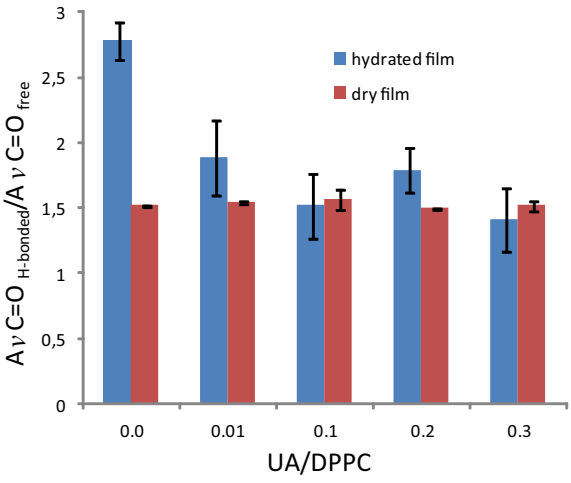

Fig. 6. The relative amount of H-bonding to the lipid C = O groups at different UA content, indicated by the ratio between the two fitted band components of the ester carbonyl stretching bands.

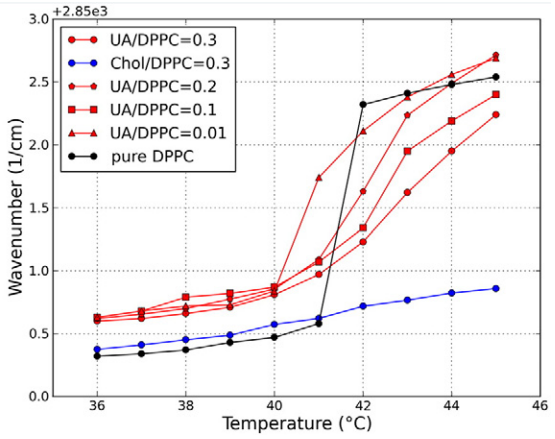

Fig. 7. Symmetric CH_2 stretching band position as a function of temperature in 20 wt% fully hydrated DPPC systems with different UA loading. For comparison, the termogram (blue line)for DPPC containing cholesterol (Chol/DPPC = 0.3 molar ratio) is also included.

[32,33]. At different UA content, a broadened gel-to-liquid crystalline phase can be observed. For higher UA concentration (UA/DPPC = 0.1-0.3) the phase transition temperature (T_m), determined as the midpoint of the melting curves, is also shifted towards higher values. Above T_m no significant increase in the proportion of *gauche* isomers of acyl chains with respect to the pure lipid (UA/DPPC = 0, black line) can be observed. Compared to the effect of cholesterol (Chol/DPPC 0.3 mol/mol, blue line), which abolish completely the main transition and hidden the formation of *gauche* conformers, a different type and mechanism of host-guest interaction between DPPC and UA versus DPPC and cholesterol has evidenced.

4. Discussion

Ursolic acid, being a non water-soluble molecule, tends to locate inside the DPPC bilayers. However, it has two polar groups at its both ends as shown in Fig. 8A. In fact UA is not a plain molecule, but is rather an elongated, roughly a rod-shaped one. As a first approximation, the *ab initio* calculation (with Gaussian 03) has revealed that its director tends to be perpendicular to that of the lipid molecule. This configuration originates from the van der Waals type interaction between the carbonyl group of the lipid and the –OH group of UA. In this work we do not intend to give a detailed theoretical calculation, but we believe that this orientation is the key to understand the peculiar structural formations in the presence of UA. The other end of the molecule is placed to the polar head group region of another lipid. Presumably, the carboxyl group points to "outside" (e.g. to the hydrated region of layer). The UA is mainly hydrophobic, so it must emerge below the head group region of the surrounding lipid molecules as demonstrated in Fig. 8B. Here, we must recall with the IR observation showing to two overlapped bands (at 1691 cm^{-1} and at 1711 cm^{-1}) indicating the aggregation/dimerization of UA's. So, we can conclude that the embedding of UA occurs with two alternative manners: single molecules or aggregation of them are present. The outer surface of UA is a local interfacial region which may be coated by the choline groups of head regions of further lipids enclosing the guest molecule at its both long sides. The consequence of this arrangement is the loss in the 'secondary hydration shell' of the lipids at the interfacial region of the bilayers. Even more, an anomalous change in the antisymmetric C-N stretching frequencies of choline groups were observed by IR spectroscopy. These all spectral changes, however, do not show any concentration dependence above UA/DPPC = 0.1 ratio, indicating that the embedding of UA molecules is uniform. It takes place locally, and only its relative abundance results in different lyotropic phases with different nanostructures and morphologies.

The consequence of this conception is the significant geometrical deformation of the parallel arrangement of lipids, whereby the curvature of interfacial surface of lipid layers can increase widely (see the meaning of φ in Fig. 8B). In the temperature domain of gel phase the actual geometrical form of "lipid-rafts" associated with UA turns into conical form and the self assembly results in the hexagonal structure. If the ratio of UA increases further, the formation of cubic structure is also favoured as it was indicated by SAXS and observed by FF-TEM. Here, we refer to the results of temperature dependent SAXS measurement, thus the layer structure is still present at high concentration of UA in the temperature domain above the chain melting. This structural characteristic can be explained by the significant expansion in the acyl chain cross-sectional area of each lipid molecule which is increased from 0.4 to 0.7 nm^2 whereby the actual geometrical form of associated UA and lipids became cylindrical, supporting the bilayer formation.

5. Conclusion

The ability of UA to induce non-bilayer structures in lipids must be related to their strong biological effect observed in many living organisms. As UA molecules present in several spices and shells of fruits, presumably these molecules play an important role in the defensive mechanisms of plants on molecular level. Beside the numerous beneficial effects of UA revealed in medical field, their impact to modify the effective shape of lipids can utilize in liposomal formulations. For the latter statement we have provided convincing experimental physicochemical results in this work.

Acknowledgement

The authors thank Teréz Kiss for the FF-TEM investigations. Part of this work was supported by the János Bolyai Research Scholarship of the Hungarian Academy of Sciences. Financial support by the Hungarian Scientific Research Fund (OTKA, Hungary) and the National Innovation Office (NIH, Hungary) under grant agreement CNK-81056 is gratefully acknowledged.

Appendix A. Supplementary data

Supplementary data to this article can be found online at http://dx.doi.org/10.1016/j.bbamem.2015.01.010.

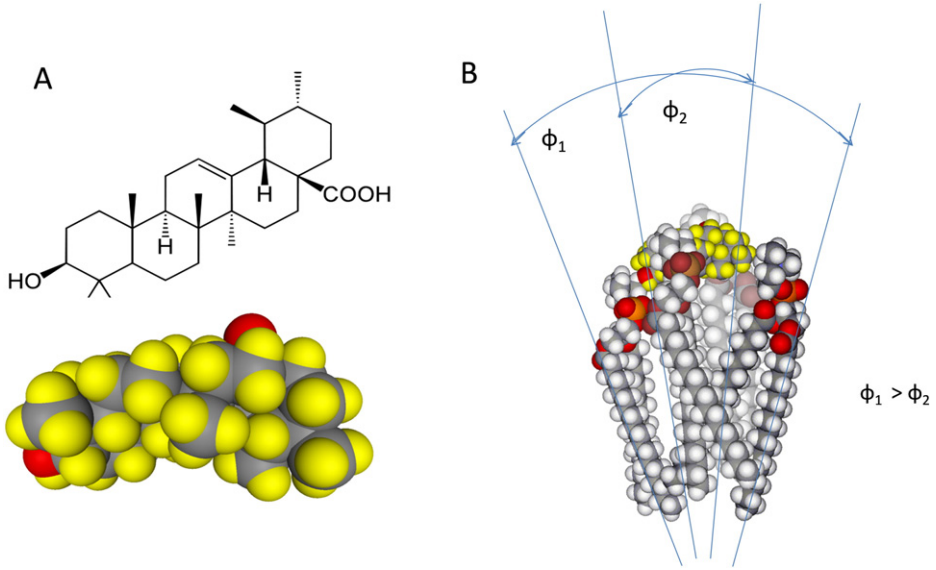

Fig. 8. Ursolic acid (A) and the conical shape of group of lipids around ursolic acid (B).

References

[1] J. Liu, Oleanolic acid and ursolic acid: Research perspectives, J. Ethnopharmacol. 100 (2005) 92–94. http://dx.doi.org/10.1016/j.jep.2005.05.024.

[2] K.W. Tan, Y. Li, J.W. Paxton, N.P. Birch, A. Scheepens, Identification of novel dietary phytochemicals inhibiting the efflux transporter breast cancer resistance protein (BCRP/ABCG2), Food Chem. 138 (2013). http://dx.doi.org/10.1016/j.foodchem.2012.12.021.

[3] T. Nabekuraa, T. Yamakia, T. Hiroia, K. Uenoa, S. Kitagawab, Inhibition of anticancer drug efflux transporter P-glycoprotein by rosemary phytochemicals, Pharmacol. Res. 61 (2010) 259–263. http://dx.doi.org/10.1016/j.phrs.

[4] J.Z. Shan, Y.Y. Xuan, S.Q. Ruan, M. Sun, Proliferation-inhibiting and Apoptosis-Inducing Effects of Ursolic Acid and Oleanolic Acid on Multi-Drug Resistance Cancer Cells in Vitro, Chin. J. Integr. Med. 17 (2011) 607–611. http://dx.doi.org/10.1007/s11655-011-0815-y.

[5] V.R. Yadav, S. Prasad, B. Sung, R. Kannappan, B.B. Aggarwal, Targeting Inflammatory Pathways by Triterpenoids for Prevention and Treatment of Cancer, Toxins 2 (2010) 2428–2466.

[6] H.B. Nair, B. Sung, V.R. Yadav, R. Kannappan, M.M. Chaturvedi, B.B. Aggarwal, Delivery of antiinflammatory nutraceuticals by nanoparticles for the prevention and treatment of cancer, Biochem. Pharmacol. 80 (2010) 1833–1843. http://dx.doi.org/10.1016/j.bcp.

[7] M.K. Shanmugam, X. Dai, A.P. Kumar, B.K.H. Tan, G. Sethi, A. Bishayee, Ursolic acid in cancer prevention and treatment: Molecular targets, pharmacokinetics and clinical studies, Biochem. Pharmacol. 85 (2013) 1579–1587. http://dx.doi.org/10.1016/j.bcp.2013.03.006.

[8] Z. Zhu, Z. Qian, Z. Yan, C. Zhao, H. Wang, G. Ying, A phase I pharmacokinetic study of ursolic acid nanoliposomes in healthy volunteers and patients with advanced solid tumors, Int. J. Nanomedicine 8 (2013) 129–136. http://dx.doi.org/10.2147/IJN.S38271.

[9] G. Cevc, D. Marsh, Phospholipid bilayers: physical principles and models, Cell Biology: A series of Monograph, vol. 5, John Wiley and Sons Ltd, 1987.

[10] P. Yeagle, Membrane models and model membranes, The membranes of cells, Orlando Academic Press, 1987. 43–66.

[11] J.J. Prades, O. Vögler, R. Alemany, M. Gomez-Florit, S.S. Funari, V. Ruiz-Gutiérrez, F. Barceló, Plant pentacyclic triterpenic acids as modulators of lipid membrane physical properties, Biochim. Biophys. Acta 1808 (2011) 752–760. http://dx.doi.org/10.1016/j.bbamem.2010.12.007.

[12] S.K. Han, Y. Ko, S.J. Park, I.J. Jin, Y.M. Kim, Oleanolic Acid and Ursolic Acid Stabilize Liposomal Membranes, Lipids 32 (1997) 769–773.

[13] H.I. Chang, M.K. Yeh, Clinical development of liposome-based drugs: formulation, characterization, and therapeutic efficacy, Int. J. Nanomedicine 7 (2012) 49–60. http://dx.doi.org/10.2147/IJN.S26766.

[14] C. Demetzos, Differential Scanning Calorimetry (DSC): a tool to study the thermal behavior of lipid bilayers and liposomal stability, J. Liposome Res. 18 (2008) 159–173. http://dx.doi.org/10.1080/08982100802310261.

[15] A. Guinier, G. Fournet, Small-angle scattering of X-rays, Wiley, New York, 1955.

[16] L.J. Lis, P.J. Quinn, The Application of Synchrotron X-radiation for the Study of Phase Transitions in Lipid Model Membrane Systems, J. Appl. Crystallogr. 24 (1991) 48–60.

[17] H.W. Meyer, W. Richter, Freeze-fracture studies on lipids and membranes, Micron 32 (2001) 615–644.

[18] R.N.A.H. Lewis, R.N. McElhaney, The structure and organization of phospholopid bilayers as revealed by infrared, spectroscopy, Chem. Phys. Lipids 96 (1998) 9–21.

[19] Z.D. Schultz, I.W. Levin, Vibrational Spectroscopy of Biomolecules, Annu. Rev. Anal. Chem. 4 (2011) 343–366.

[20] M.A. Singh, S.S. Ghosh, J.R. Shannon, A direct method of beam-height correction of small-angle X-ray scattering, J. Appl. Crystallogr. 26 (1993) 787–794.

[21] M.J. Frisch, G.W. Trucks, H.B. Schlegel, G.E. Scuseria, M.A. Robb, J.R. Cheeseman, J.A. Montgomery, T. Vreven, K.N. Kudin, J.C. Burant, J.M. Millam, S.S. Iyengar, J. Tomasi, V. Barone, B. Mennucci, M. Cossi, G. Scalmani, N. Rega, G.A. Petersson, H. Nakatsuji, M. Hada, M. Ehara, K. Toyota, R. Fukuda, J. Hasegawa, M. Ishida, T. Nakajima, Y. Honda, O. Kitao, H. Nakai, M. Klene, X. Li, J.E. Knox, H.P. Hratchian, J.B. Cross, V. Bakken, C. Adamo, J. Jaramillo, R. Gomperts, R.E. Stratmann, O. Yazyev, A.J. Austin, R. Cammi, C. Pomelli, J.W. Ochterski, P.Y. Ayala, K. Morokuma, G.A. Voth, P. Salvador, J.J. Dannenberg, V.G. Zakrzewski, S. Dapprich, A.D. Daniels, M.C. Strain, O. Farkas, D.K. Malick, A.D. Rabuck, K. Raghavachari, J.B. Foresman, J.V. Ortiz, Q. Cui, A.G. Baboul, S. Clifford, J. Cioslowski, B.B. Stefanov, G. Liu, A. Liashenko, P. Piskorz, I. Komaromi, R.L. Martin, D.J. Fox, T. Keith, M.A. Al-Laham, C.Y. Peng, A. Nanayakkara, M. Challacombe, P.M.W. Gill, B. Johnson, W. Chen, M.W. Wong, C. Gonzalez, J.A. Pople, Gaussian 03, Revision E.01, Gaussian, Inc., Wallingford, CT, 2004.

[22] A.D. Becke, Density-functional thermochemistry.III. The role of exact exchange, J. Chem. Phys. 98 (1993) 5648–5652.

[23] A. Bóta, T. Drucker, M. Kriechbaum, Zs. Pálfia, G. Réz, Layer Formations of Dipalmitoylphosphatidylcholine Liposomes in the Pretransition Range, Langmuir 15 (1999) 3101–3108.

[24] Á. Oszlánczi, A. Bóta, Sz. Berényi, E. Klumpp, Structural and morphological changes in bacteria-membrane mimetic DPPE/DPPGwater systems induced by sulfadiazine, Colloids Surf. B: Biointerfaces 76 (2010) 519–528.

[25] A.C.T. Teixeira, A.C. Fernandes, A.R. Garcia, L.M. Ilharco, P. Brogueira, A.M.P.S. Goncalves da Silva, Microdomains in mixed monolayers of oleanolic and stearic acids: thermodynamic study and BAM observation at the air–water interface and AFM and FTIR analysis of LB monolayers, Chem. Phys. Lipids 149 (2007) 1–13.

[26] S. Binduja, P.K.S. Visen, D.P. Agarwal, Ursolic acid isolated from Eucalyptus tereticornis protects against ethanol toxicity in isolated rat hepatocytes, Phytother. Res. 14 (2000) 163–166.

[27] J.L.R. Arrondo, F.M. Goñi, J.M. Macarulla, Infrared spectroscopy of phosphatidylcholines in aqueous suspension. A study of the phosphate group vibrations, Biochim. Biophys. Acta 795 (1984) 165–168.

[28] M. Arczewska, D.M. Kaminski, E. Gorecka, D. Pociecha, E. Roj, A. Sawinska-Brych, M. Gagos, The molecular organization of prenylated flavonoid xanthohumol in DPPC multibilayers: X-ray diffraction and FTIR spectroscopic studies, Biochim. Biophys. Acta 1828 (2013) 213–222.

[29] P.T.T. Wong, H.H. Mantsch, High-pressure infrared spectroscopic evidence of water binding sites in 1,2-diacyl phospholipids, Chem. Phys. Lipids 46 (1988) 213–224.

[30] R.N.A.H. Lewis, R.N. McElhaney, W. Pohle, H.H. Mantsch, Components of the carbonyl stretching band in the infrared spectra of hydrated 1,2-diacylglycerol bilayers: A reevaluation, Biophys. J. 67 (1994) 2367–2375.

[31] S. Berenyi, J. Mihaly, S. Kristyan, L. Naszalyi Nagy, J. Telegdi, A. Bota, Thermotropic and Structural Effects of Poly(malic acid) on Fully Hydrated Multilamellar DPPC–Water Systems, Biochim. Biophys. Acta Biomembr. 1828 (2013) 661–669. http://dx.doi.org/10.1016/j.bbamem.2012.09.023.

[32] R.N.A.H. Lewis, R.N. McElhaney, Vibrational Spectroscopy of Lipids, in Handbook of Vibrational Spectroscopy, in: J.M. Calmers, P. Griffiths (Eds.), John Wiley &Sons, Inc., 2001, pp. 3784–3801.

[33] R.N.A.H. Lewis, R.N. McElhaney, Membrane lipid phase transitions and phase organization studied by Fourier transform infrared spectroscopy, Biochim. Biophys. Acta 1828 (2013) 2347–2358.